Research Article | Open Access

Microstructures

Li *et al. Microstructures* **2026**, *6*, 2026027 **DOI:**10.20517/microstructures.2025.92

Ultrahigh piezoelectric response in $Pb(Ni_{1/3}Nb_{2/3})O_3$-$PbZrO_3$-$PbTiO_3$ ceramics

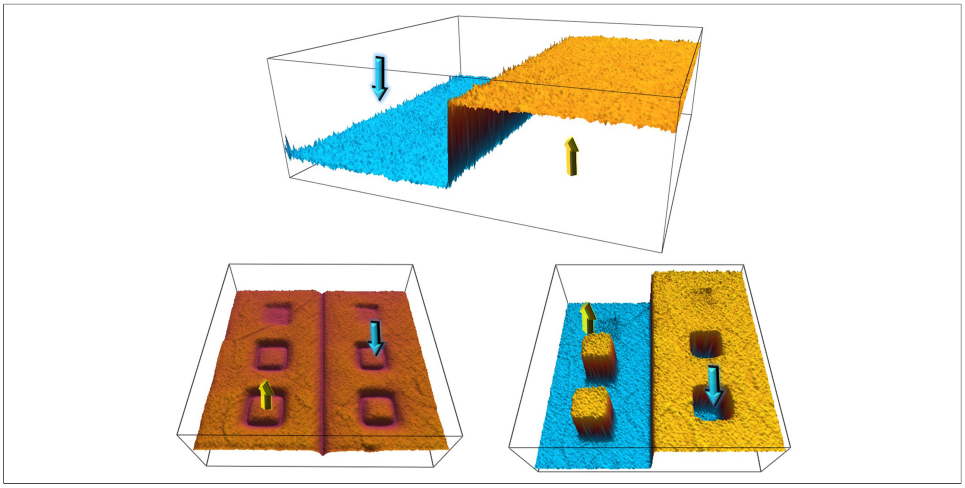
Kai Li[1,#], Qian Wang[2,#], Yiqiao Zhou[3], Zehui Yang[1], Zuwen Zeng[1], Yihui An[1], Lang Bian[2], Zhenting Zhao[1], Haijuan Mei[1], Duoduo Zhang[1], Weiping Gong[1], Xudong Qi[4], Limei Zheng[5]

Keywords:
Piezoelectric ceramics, PNN-PZ-PT, ultrahigh piezoelectricity, domain structure and evolution

Citation: Li, K.; Wang, Q.; Zhou, Y.; Yang, Z.; Zeng, Z.; An, Y.; Bian, L.; Zhao, Z.; Mei, H.; Zhang, D.; Gong, W.; Qi, X.; Zheng, L. Ultrahigh piezoelectric response in $Pb(Ni_{1/3}Nb_{2/3})O_3$-$PbZrO_3$-$PbTiO_3$ ceramics. *Microstructures* **2026**, *6*, 2026027. https://dx.doi.org/10.20517/microstructures.2025.92

Received: 26 Jun 2025 **First Decision:** 28 Aug 2025 **Revised:** 28 Sep 2025 **Accepted:** 20 Oct 2025 **Published:** 12 Mar 2026

Academic Editor: Jie Wang
Copy Editor: Ping Zhang
Production Editor: Ping Zhang



Abstract

To meet the escalating demands for high-performance piezoelectric materials in fields such as modern medical diagnostics, precision manufacturing, *etc.*, we developed a ternary $0.555Pb(Ni_{1/3}Nb_{2/3})O_3$-$0.145PbZrO_3$-$0.30PbTiO_3$ (PNN-PZ-PT) piezoelectric ceramic located at the tricritical point of rhombohedral, tetragonal and pseudocubic phases. This ceramic, with coexistence of multiple ferroelectric phases, demonstrates an ultrahigh piezoelectric coefficient d_{33} of 1190 picocoulombs per newton (pC/N) and a large relative dielectric constant ε_r of 9900. Analysis of the domain structure reveals irregular maze-like nanodomains with strong local disorder. These nanodomain structures exhibit excellent local piezoelectric response and polarization switching characteristics, thereby enhancing the alignment of polarization vectors during poling and ensuring the high stability after being poled. The tricritical point composition with disordered nanodomains can

[1]Guangdong Provincial Key Laboratory of Electronic Functional Materials and Devices, Huizhou University, Huizhou 516001, Guangdong, China.
[2]Condensed Matter Science and Technology Institute, School of Instrumentation Science and Engineering, Harbin Institute of Technology, Harbin 150080, Heilongjiang, China.
[3]School of Energy and Environmental Engineering, University of Science and Technology Beijing, Beijing 100080, China.
[4]School of Physics and Electronic Engineering, Key Laboratory for Photonic and Electronic Bandgap Materials, Ministry of Education, Harbin Normal University, Harbin 150025, Heilongjiang, China.
[5]School of Physics, Shandong University, Jinan 250100, Shandong, China.
[#]These authors contributed equally to this work.

Correspondence to: Dr. Kai Li, Prof. Weiping Gong, Guangdong Provincial Key Laboratory of Electronic Functional Materials and Devices, Huizhou University, Huizhou 516001, Guangdong, China. E-mail: kailics@hzu.edu.cn; gwp@hzu.edu.cn; Prof. Limei Zheng, School of Physics, Shandong University, Jinan 250100, Shandong, China. E-mail: zhenglm@sdu.edu.cn

significantly enhance the contribution of polarization to macroscopic piezoelectric properties, offering a promising approach for developing ceramics with superior piezoelectricity.

INTRODUCTION

Piezoelectric ceramics can interconvert mechanical and electrical energy, making them essential components in transducers and sensors for a wide range of electromechanical applications[1-5]. Among piezoceramics, $Pb(Zr, Ti)O_3$ (PZT)-based relaxor ferroelectrics are highly promising for high-performance electromechanical devices due to excellent piezoelectric properties at compositions near morphotropic phase boundary (MPB). However, given the ever-increasing demand in modern medical diagnostics and precision manufacturing, piezoelectric materials with large piezoelectric response are required. Therefore, designing and developing piezoceramics with superior piezoelectric properties has become a new urgent requirement.

To further enhance the piezoelectric activity of PZT ceramics, a highly effective strategy is to form a relaxor ferroelectric solid solution by incorporating a relaxor end-member [general formula $Pb(B', B'')O_3$, where B' represents low-valence cations such as Zn^{2+}, Mg^{2+}, Ni^{2+}, In^{3+}, or Sc^{3+}, and B" denotes high-valence cations such as Nb^{5+}, Ta^{5+}, or W^{6+}] into normal PZT ferroelectrics to construct an MPB region over a broad composition range. In this region, the coexistence of two or more ferroelectric phases flattens the free-energy density profile associated with polarization rotation between different ferroelectric phases and is responsible for the excellent piezoelectricity[6-10].

In addition, it has been found that the intrinsic chemical/compositional heterogeneity on the atomic scale can be engineered for the $Pb(B', B'')O_3$-PZT relaxor ferroelectric solid solutions due to the enhanced local disordered arrangement of B-site heterovalent cations, and the local structural heterogeneity, or polar nanoregions (PNRs) can reduce energy barrier and then promote polarization rotation induced by external field, leading to the greatly enhanced piezoelectric properties and dielectric relaxation behavior[11-18]. Therefore, designing PZT-based relaxor ferroelectric ceramics with local heterogeneous structures is highly beneficial and crucial for achieving ultrahigh piezoelectric response.

It has been reported that $Pb(Ni_{1/3}Nb_{2/3})O_3$-$PbZrO_3$-$PbTiO_3$ (PNN-PZ-PT) ceramics possess a complex phase composition, which may include rhombohedral (R), tetragonal (T), pseudocubic (P), and cubic (C) structures[8,19,20]. Recent studies indicate that the macroscopic properties of PNN-PZ-PT ceramics are strongly influenced by the microstructure. For instance, ultrahigh piezoelectric coefficients d_{33} have been achieved in PNN-PZ-PT ceramics with a multiphase coexistent composition[8,13]. Additionally, T-phase PNN-PZ-PT ceramics typically exhibit high Curie temperature (T_c), while R-phase compositions demonstrate a favorable balance between d_{33} and T_c[19-21]. Specifically, the PNN-PZ-PT ceramics are characterized by a microscopically dispersed nano-domain morphology, which plays a critical role in determining the macroscopic electric properties[22-25]. It is widely recognized that domain switching and polarization reversal under external stimuli are fundamental mechanisms underlying piezoelectricity. Consequently, systematically and deeply investigating the polarization configuration and electric field-induced polarization switching in PNN-PZ-PT ceramics, including the polarization orientation distribution, local piezoelectric response intensity, and polarization retention under external fields, is essential for understanding the structure-property relationship of high-performance PNN-PZ-PT ceramics.

In this work, the tricritical point composition 0.555PNN-0.145PZ-0.30PT ceramics with ultrahigh d_{33} were designed and successfully fabricated by improved solid-state reaction method. The dielectric, ferroelectric, and piezoelectric properties of the synthesized ceramics were systematically investigated. Furthermore, the

nanoscale domain structures, local piezoelectric response and polarization switching behavior of the PNN-PZ-PT ceramics were systematically and deeply characterized and analyzed by piezoelectric force microscopy (PFM) to elucidate the underlying physical mechanisms responsible for its outstanding piezoelectricity.

EXPERIMENTAL PROCEDURE

The 0.555PNN-0.145PZ-0.30PT ceramics were synthesized via an improved solid-state reaction method. High-purity starting materials, including TiO_2 (Aladdin, 99.8%), Nb_2O_5 (Aladdin, 99%), ZrO_2 (Aladdin, 99%), 0.5 mol% excess NiO (Aladdin, 99%), and 1.5 mol% excess PbO (Aladdin, 99.9%), were sequentially processed according to the procedure of weighing, mixing, and ball-milling in alcohol for 24 h. After ball-milling, the mixed powder was dried at 100 °C and calcined at 750 °C for 2 h to obtain PNN-PZ-PT powder, which was then ball-milled again for 24 h and dried. Finally, the powder was pressed into disc-shaped pellets (13 mm in diameter and 1 mm in thickness) under a pressure of 250 MPa and sintered in air at 1,250 °C for 2.5 h.

The crystalline phase structure of the PNN-PZ-PT ceramics was measured using an X-ray diffraction (XRD; MiniFlex 600, Rigaku, Japan). The microstructures of the cross-section and polished surface after annealing treatment were observed using a scanning electron microscopy (SEM; VEGA3/XUM, TESCAN, USA). The domain structures and polarization switching were observed using a PFM (MFP-3D Origin+, Asylum Research, USA). The ceramics were poled using a 15 kV/cm direct current (DC) electric field at room temperature for 30 min, followed by characterization of the electro-mechanical properties. The piezoelectric coefficient was measured using a piezo d_{33} meter (ZJ-4A, Institute of Acoustics, Chinese Academy of Sciences, China), while temperature-dependent dielectric spectra were acquired via an LCR meter (E4980A, Agilent, USA). Ferroelectric hysteresis loops were recorded using a Premier II system (Radiant Technologies Inc., USA) combined with a temperature control system.

RESULTS AND DISCUSSION

Phase structure and microstructure morphology

Figure 1A illustrates the phase diagram of PNN-PZ-PT systems[8]. The selected ceramic composition of 0.555PNN-0.145PZ-0.30PT is located at the tricritical point of R, T, and P phases. Figure 1B shows the XRD patterns of unpoled and 15 kV/cm DC electric field-poled PNN-PZ-PT ceramics at room temperature. The ceramics exhibit a pure perovskite structure free of pyrochlore or secondary phases. Moreover, both the unpoled and poled samples exhibit a broadened single (200) peak at approximately 45° due to the superposition of peaks from the triple-phase structure[19,26]. To quantify the phase fractions and lattice parameters of PNN-PZ-PT ceramic, the Rietveld refinement of the XRD pattern of the poled ceramic was performed. The corresponding results, along with the refinement parameters, are provided in Supplementary Figure 1 and Supplementary Table 1 of the Supplementary Materials. The SEM images of the cross-section and polished surface after annealing treatment of PNN-PZ-PT ceramics are shown in Figure 1C and D. The ceramics exhibit well-aligned and uniform grain arrangement with no obvious pores, indicating that the ceramics are fully reacted and well-sintered, ultimately resulting in a high density. The calculated average grain size is 3.4 μm with a normal distribution by counting more than 200 grains.

Electrical characteristics

The PNN-PZ-PT ceramics were poled using a 15 kV/cm DC electric field at room temperature for 30 min. After aging for more than 24 h, the piezoelectric coefficients of multiple ceramic samples, as well as the same sample aged for different durations, were measured at room temperature using a d_{33} piezometer, showing an excellent value of 1190 ± 15 picocoulombs per newton (pC/N). Subsequently, the temperature-dependent

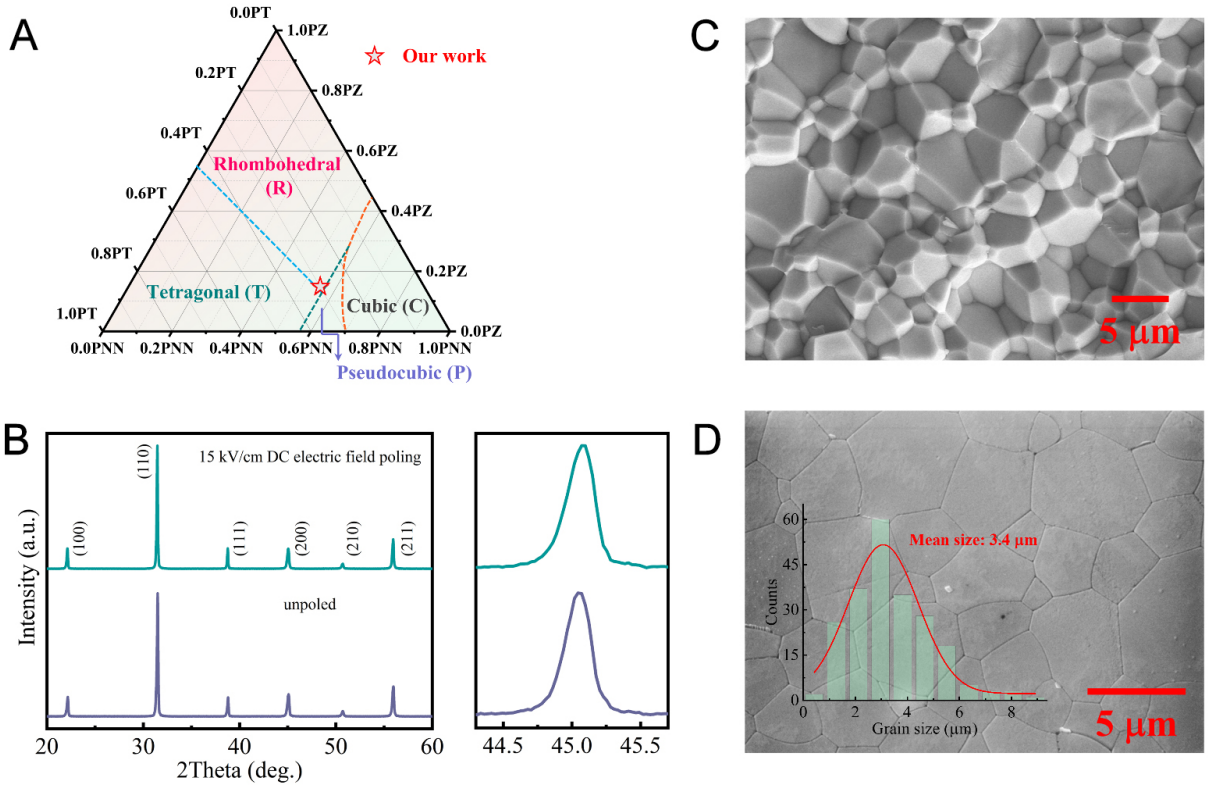


Figure 1. (A) Phase diagram of PNN-PZ-PT ternary system (reproduced from Ref.8)[8]; (B) XRD patterns and SEM images of (C) the cross-section and (D) polished surface after annealing treatment for 0.555PNN-0.145PZ-0.30PT ceramics. SEM: Scanning electron microscopy; XRD: X-ray diffraction; PNN-PZ-PT: $Pb(Ni_{1/3}Nb_{2/3})O_3$-$PbZrO_3$-$PbTiO_3$.

dielectric constant of the poled PNN-PZ-PT ceramic was also investigated, as shown in Figure 2A, and a high room temperature dielectric constant (ε_r) of 9900 was obtained. According to the thermodynamic theory, there exists a classical relationship $d = 2PQ\varepsilon$, where P and ε stand for the spontaneous polarization intensity and the dielectric constant, respectively. Q denotes the electrostriction coefficient, which is usually assumed to be constant in the same system. Therefore, it can be inferred that the exceptional d_{33} value observed in PNN-PZ-PT ceramics primarily originates from the elevated relative dielectric constant. Furthermore, this ultrahigh room-temperature dielectric permittivity renders this material system particularly advantageous for applications in low-frequency medical ultrasonic imaging array transducers[8].

From Figure 2A, it can also be observed that the PNN-PZ-PT ceramic exhibits a typical dielectric relaxation behavior, i.e., a broad dielectric peak (diffuse phase transition) at maximum dielectric permittivity temperature T_m and a shift of the T_m value to higher temperatures as the frequency increases (frequency dispersion). To further investigate the dielectric relaxation characteristic of the PNN-PZ-PT ceramic, the plot of $\ln(1/\varepsilon - 1/\varepsilon_m)$ versus $\ln(T - T_m)$ was fitted by the modified Curie-Weiss law[27]:

$$\frac{1}{\varepsilon} - \frac{1}{\varepsilon_m} = \frac{(T - T_m)^\gamma}{C} \quad (1)$$

where ε_m and C are maximum dielectric permittivity and Curie-Weiss-like constant, respectively, and γ ($1 < \gamma < 2$) describes the diffuseness degree of the phase transition. Usually, $\gamma = 1$ and $\gamma = 2$ represent the ideal normal and relaxor ferroelectrics, respectively. The fitting value of γ is 1.64 for the PNN-PZ-PT ceramic, indicating a strong diffuseness degree, as seen in Figure 2B. Moreover, the frequency-induced T_m deviation, expressed as $T_m = T_{m,\,100\,kHz} - T_{m,\,100\,Hz}$, can be used to quantitatively evaluate the frequency dispersion behavior of relaxor ferroelectrics; the bigger the T_m, the stronger the frequency dispersion. From Figure 2C, the T_m

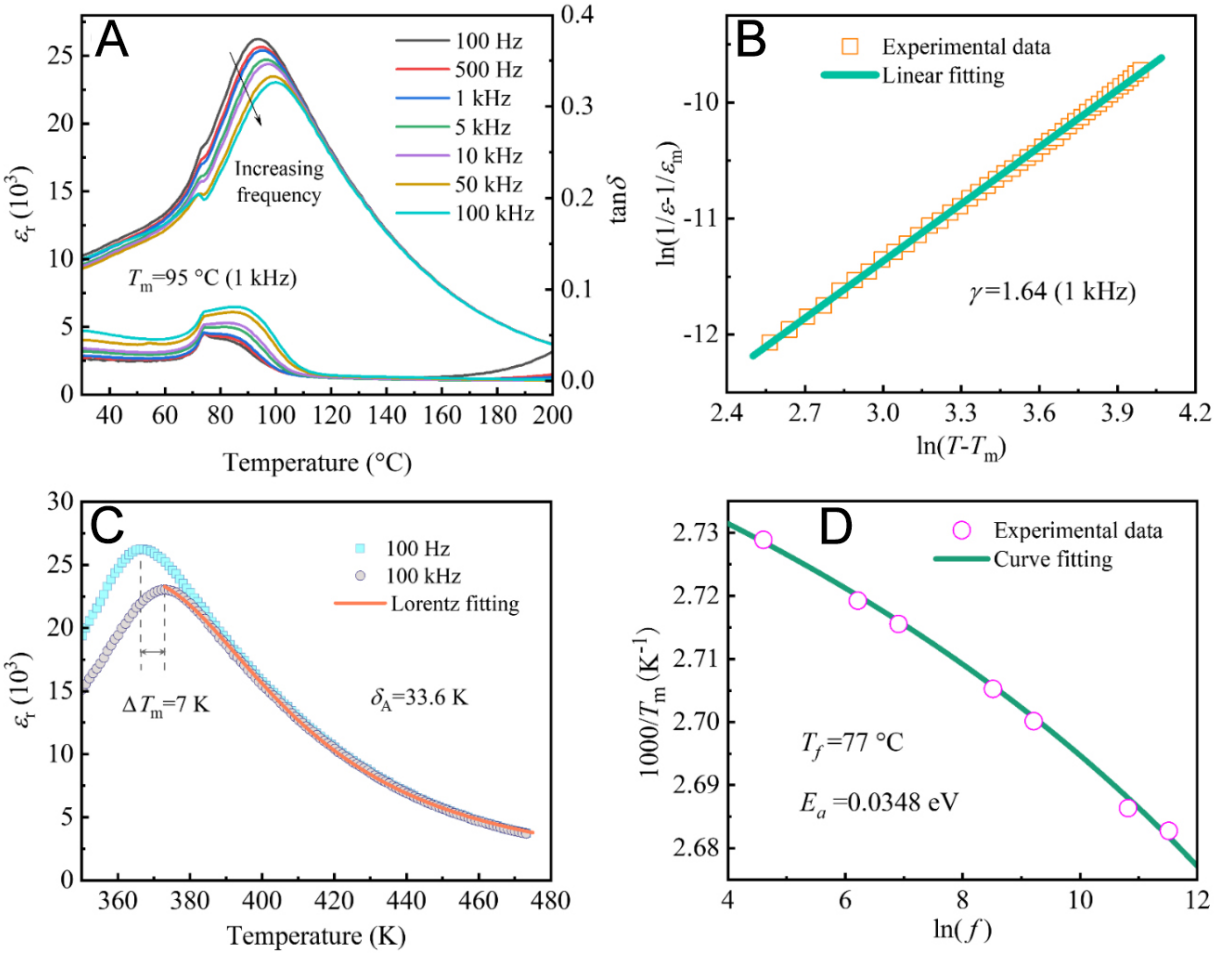


Figure 2. (A) The temperature- and frequency-dependent ε_r and tanδ, (B) modified Curie-Weiss law, (C) Lorentz-type relation, and (D) Vogel-Fulcher fitting results for the 0.555PNN-0.145PZ-0.30PT ceramics.

value of 7 K was obtained, which is bigger than that of classic $Pb(Mg_{1/3}Nb_{2/3})O_3$-$PbTiO_3$ (PMN-PT) relaxor ferroelectric single crystal with R phase[28].

Furthermore, the Lorentz quadratic relationship provides an effective analytical framework for quantifying the degree of phase transition diffuseness near the T-C phase transition temperature T_m, as follows[29]:

$$\frac{\varepsilon_A}{\varepsilon} - 1 = \frac{(T - T_A)^2}{2\delta_A^2} \tag{2}$$

where the fitting parameters T_A and ε_A are the temperature and the value of ε at the temperature of T_A. The δ_A is the half width of permittivity peak at 2/3 of the maximum and characterizes the diffuseness degree of phase transition, which can be achieved from the curve fitting, as shown in Figure 2C. The fitting results demonstrate that the temperature dependence of ε_r above T_m follows the Lorentz quadratic relationship, yielding a diffuseness parameter δ_A = 33.6 K, which is higher than those reported for PMN-PT and $Pb(In_{1/2}Nb_{1/2})O_3$-$Pb(Mg_{1/3}Nb_{2/3})O_3$-$PbTiO_3$ (PIN-PMN-PT) single crystals[28]. This observed phenomenon of a larger δ_A value and stronger dielectric diffuseness behavior can be attributed to a more significant local structural heterogeneity in the PNN-PZ-PT ceramics when compared to the reference materials.

The temperature dependence of the ε_r [Figure 2A] exhibits a distinct peak at T_m = 95 °C (measured at 1 kHz), corresponding to the ferroelectric-to-paraelectric phase transition. This observation aligns with the

compositional design incorporating 0.555PNN, as the intrinsic Curie temperature of pure PNN ceramics is significantly lower (T_c ~ 120 °C) compared with that of $PbZrO_3$ (T_c ~ 230 °C) and $PbTiO_3$ (T_c ~ 490 °C)[30]. Additionally, a dielectric anomaly at the temperature of 74 °C, corresponding to the depolarization temperature (T_d), was found in the dielectric temperature spectrum of the poled PNN-PZ-PT ceramic. For relaxor ferroelectrics, the frequency dispersion behavior can be given by the Vogel-Fulcher law[31,32]:

$$f = f_0 \exp\left[\frac{-E_a}{k\left(T_m - T_f\right)}\right] \tag{3}$$

where f, f_0, k and E_a are the test frequency, Debye frequency, Boltzmann constant and activation energy, respectively. T_f is the static freezing temperature at which the macroscopic long-range ordered ferroelectric domains will split into nanoscale disordered domain structures accompanied by abrupt electric performance changes. E_a represents the activation energy for polarization fluctuation within an isolated cluster, resulting from the development of short-range order. A higher E_a indicates stronger interactions between adjacent PNRs[32,33]. As shown in Figure 2D, the fitted parameter E_a of the ternary 0.555PNN-0.145PZ-0.30PT ceramic is around 0.0348 eV, which is comparable to those of the ternary 0.26PIN-0.47PMN-0.27PT (0.038 eV) and 0.26PIN-0.44PMN-0.30PT (0.0331 eV) single crystals[34], but significantly higher than those of the binary 0.67PMN-0.33PT (0.008 eV)[4] and 0.71PMN-0.29PT (0.0152 eV)[34] single crystals. This indicates strong interactions between the polar nanodomains in the ternary 0.555PNN-0.145PZ-0.30PT piezoelectric ceramic. Additionally, the fitted parameter T_f of the poled PNN-PZ-PT ceramic obtained from Equation 3 is 77 °C, which is close to the T_d (74 °C) [Figure 2A], further confirming that the depolarization at T_d is caused by the decomposition of DC electric field-induced long-range ordered ferroelectric domains into short-range disordered nanodomains.

Figure 3A depicts the polarization-electric field (*P-E*) hysteresis loops of PNN-PZ-PT ceramic measured at a frequency of 1 Hz and room temperature. At 5 kV/cm, the loops exhibit a rectangular profile characteristic of ferroelectric domain switching, with full saturation achieved at 10 kV/cm, which indicates facile polarization rotation under external electric fields. Figure 3B presents the variation of saturated polarization (P_s) and remnant polarization (P_r) of PNN-PZ-PT ceramics with the test electric field. When the test electric field is 15 kV/cm, the P_s and P_r are 25.8 μC/cm² and 21.5 μC/cm², respectively. In addition, compared with some other representative high piezoelectric performance ceramics, the PNN-PZ-PT ceramic exhibits a smaller coercive electric field (E_c), which is 3.3 kV/cm, as shown in Table 1.

As shown in Figure 3C, the frequency-dependent E_c follows the classical Merz switching dynamics[39-41], as given by:

$$\tau \propto \frac{1}{f} \propto \exp\left(\frac{E_\alpha}{E_c}\right) \tag{4}$$

where τ represents the domain switching time, f denotes the measurement frequency, and E_a quantifies the activation electric field required for nucleation and growth of new ferroelectric domains. As shown in Figure 3D, the fitting analysis yields E_a = 43.3 kV/cm for the PNN-PZ-PT ceramic, which is lower than that of the T phase of the PNN-PZ-PT system, but comparable to those of R-phase PMN-PT (49 kV/cm)[28] and PIN-PZ-PMN-PT (40.9 kV/cm)[42]. Supplementary Figure 2 presents the frequency-dependent *P-E* loops and corresponding fitting results based on Merz's switching law for the T-phase PNN-PZ-PT ceramic and the PIN-PMN-PT system in both the MPB region and T phase. Supplementary Table 2 summarizes the E_a values obtained in this study along with those reported in the literature. Furthermore, Supplementary Figure 3 shows the fatigue performance of the PNN-PZ-PT ceramic, which exhibits excellent fatigue endurance with negligible degradation in *P-E* loops, polarization, and coercive field after 10^6 cycles.

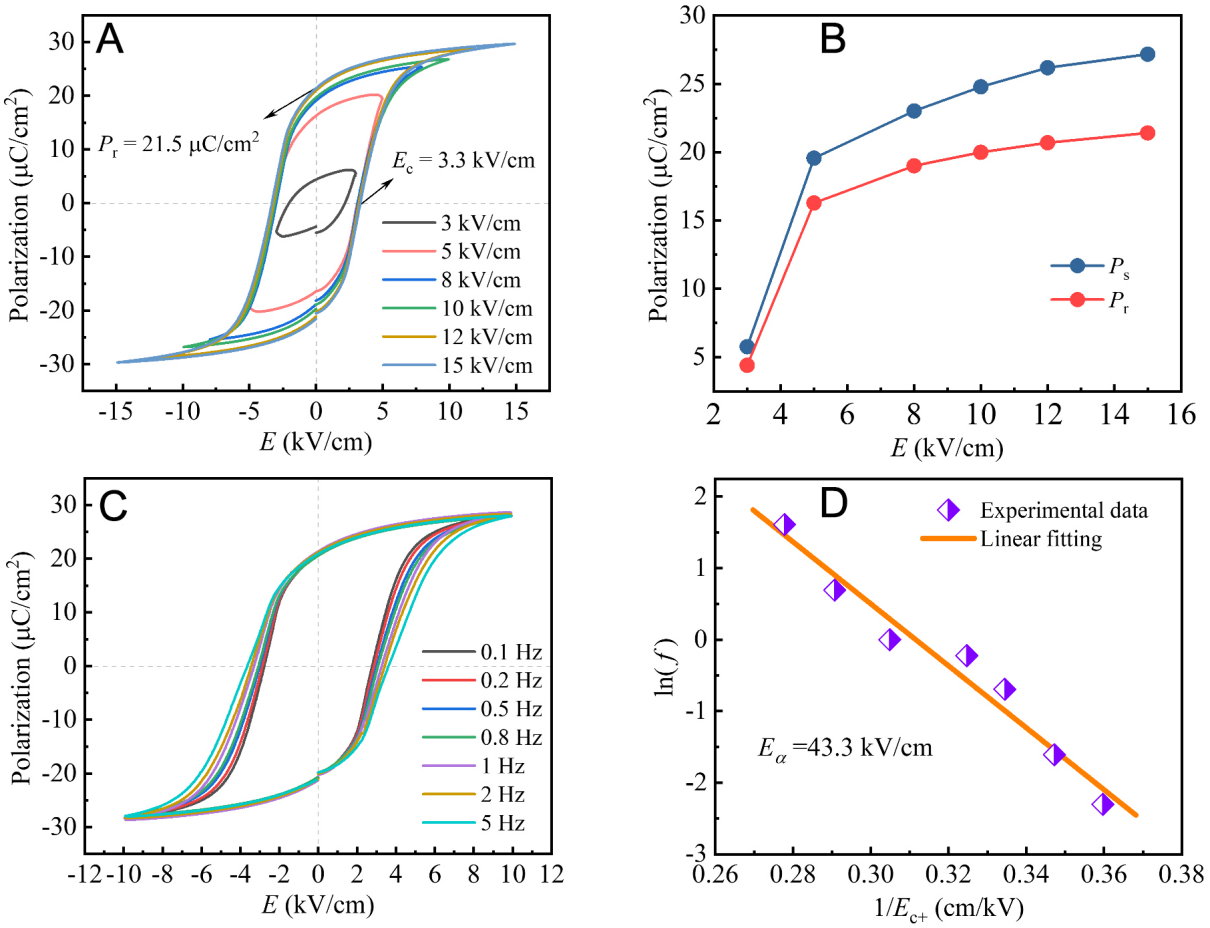


Figure 3. (A) Electric field-dependent and (C) frequency-dependent *P-E* loops; (B) Variations of P_s and P_r as a function of electric field, and (D) E_{c+} as a function of frequency for the 0.555PNN-0.145PZ-0.30PT ceramics at room temperature. *P-E*: Polarization-electric field.

Table 1. Performance comparison of several representative piezoelectric ceramics

Ceramics	d_{33} (pC/N)	ε_r	T_c (°C)	tan δ (%)	E_c (kV/cm)	References
PNN-PZ-PT	1190	9900	95	2.7	3.3	This work
PNN-PZ-PT: Sm	1130	6375	130	3.2	5.81	[35]
PMN-PT: Sm	1510	13000	89	3.5	2.3	[11]
PMN-PT-BNZ	1040	6884	123	4.2	4.5	[36]
PIN-PMN-PT: Sm	905	4292	179	3.0	7.4	[37]
KNNS-BNKH	525	1820	220	3.5	8.5	[38]

PNN-PZ-PT: $Pb(Ni_{1/3}Nb_{2/3})O_3$-$PbZrO_3$-$PbTiO_3$; PMN-PT-BNZ: $Pb(Mg_{1/3}Nb_{2/3})O_3$-$PbTiO_3$-$(Bi_{0.5}Na_{0.5})ZrO_3$; PIN-PMN-PT: $Pb(In_{1/2}Nb_{1/2})O_3$-$Pb(Mg_{1/3}Nb_{2/3})O_3$-$PbTiO_3$; KNNS-BNKH: $(K_{1-y}Na_y)(Nb_{1-z}Sb_z)O_3$-$Bi_{0.5}(Na_{1-w}K_w)_{0.5}HfO_3$.

To investigate the thermal depolarization characteristic of the high-performance PNN-PZ-PT ceramic (d_{33} = 1190 pC/N), the poled ceramics were subjected to annealing treatments at different temperatures for 0.5 h, followed by cooling to room temperature. The temperature-dependent piezoelectric response was subsequently evaluated through d_{33} measurements, with results presented in Figure 4A. The PNN-PZ-PT ceramic exhibits excellent thermal stability of its piezoelectric response, maintaining d_{33} > 1000 pC/N when the annealing temperature is below 75 °C. When the annealing temperature reaches 85 °C, the d_{33} of poled PNN-PZ-PT ceramic drops sharply to 500 pC/N, primarily due to the thermal-induced decomposition of

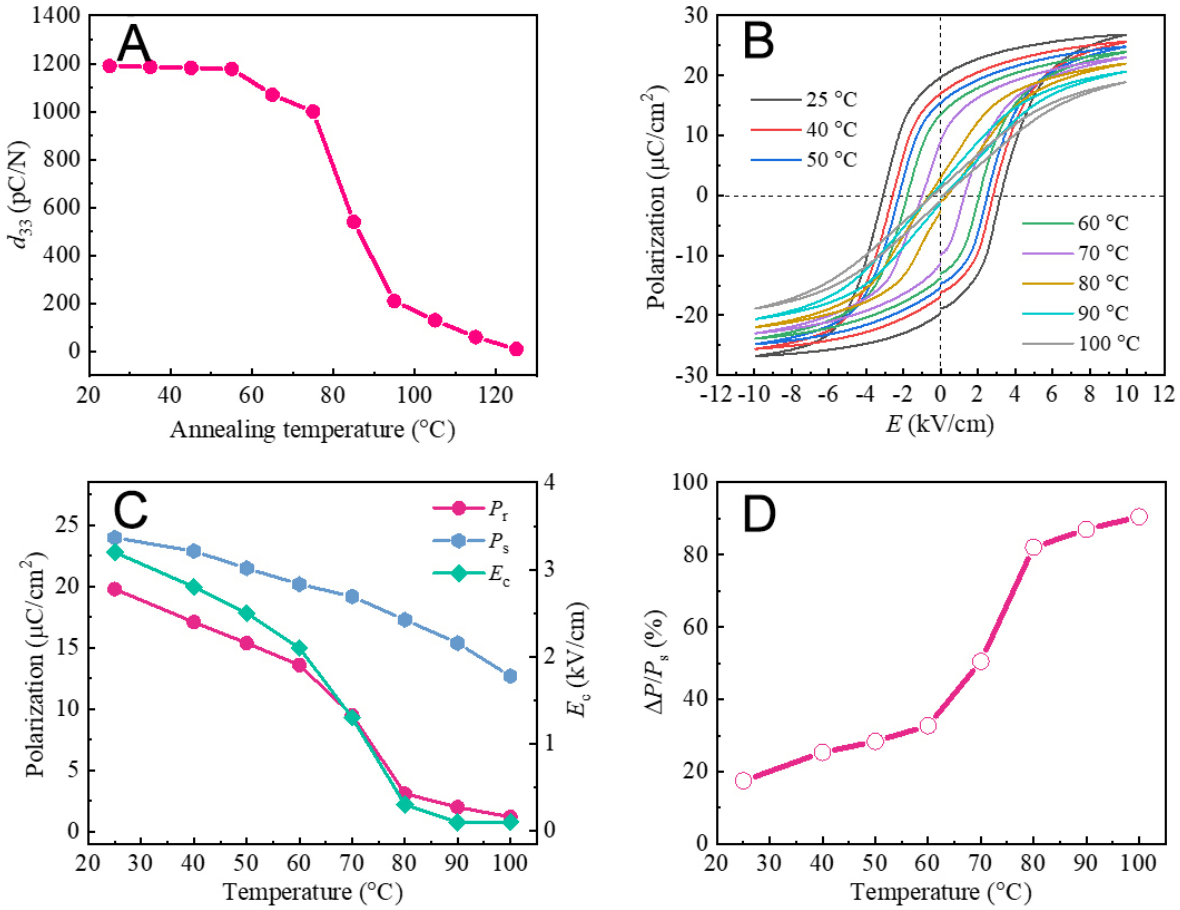


Figure 4. (A) Piezoelectric coefficient as a function of annealing temperature, (B) temperature-dependent *P-E* loops, (C) variations of P_s and P_r, and (D) change proportion in polarization as a function of temperature for the 0.555PNN-0.145PZ-0.30PT ceramics. *P-E*: Polarization-electric field.

macroscopic long-range ordered ferroelectric domains into randomly disordered domains. Elevated annealing temperatures (~100 °C) induce a phase transition from the ferroelectric T phase to C phase, manifesting severely attenuated piezoelectric activity (d_{33} ~ 100 pC/N).

Figure 4B shows the temperature-dependent *P-E* loops of the PNN-PZ-PT ceramic measured at 10 kV/cm and 1 Hz, and the ferroelectric characteristic parameters, including P_s, P_r, E_c, and change proportion in polarization ($\Delta P/P_s$, $\Delta P = P_s - P_r$), as a function of temperature are presented in Figure 4B-D. As shown in Figure 4C, the E_c of PNN-PZ-PT ceramics gradually decreases with increasing temperature. Notably, when the temperature exceeds 70 °C, the E_c drops sharply, and it is noteworthy that this measurement temperature approaches the depolarization temperature (as seen in Figure 2A), at which the macroscopic domains transition into nanoscale domain structures.

In temperature-dependent ferroelectric characterization of PNN-PZ-PT ceramics, P_r corresponds to the effective projection component of the spontaneous polarization along the electric field direction under thermal effects after the removal of the electric field, and a higher P_r reflects a greater contribution of polarization vectors to the macroscopic piezoelectric response. Notably, the gradual increase in temperature leads to a reduction in P_r, with a sharp decline observed near the depolarization temperature, as seen in Figure 4C. This confirms that the long-range ordered domain structures, induced by the measurement electric field, undergo fragmentation into nano-domain configurations under elevated temperatures.

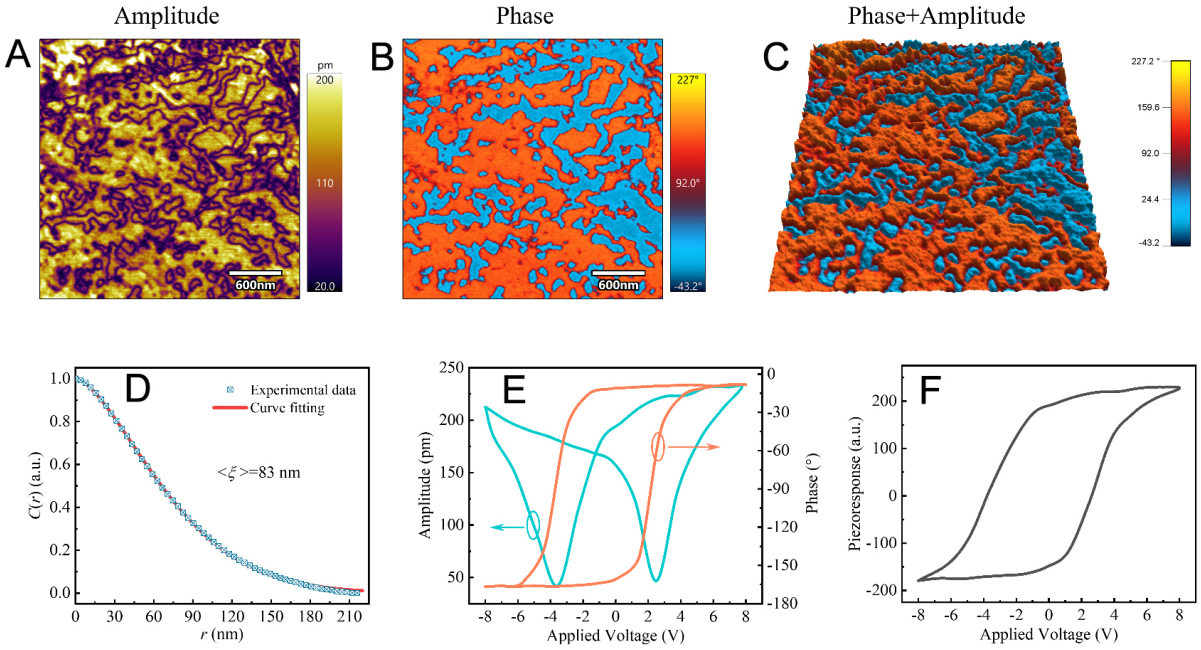


Figure 5. (A-C) PFM images with a 3 μm 3 μm region; (D) Average autocorrelation function < *C*(*r*) >; (E and F) Amplitude-voltage, phase-voltage, and local piezoresponse loop of the unpoled 0.555PNN-0.145PZ-0.30PT ceramics. PFM: Piezoelectric force microscopy.

Concurrently, the *P*-*E* loops of the PNN-PZ-PT ceramics exhibit pronounced relaxor characteristics, accompanied by an abrupt reduction in piezoelectric coefficients.

In addition, for piezoelectric materials, the polarization retention after the removal of the external electric field can be expressed by the change proportion in polarization ($\Delta P/P_s$, $\Delta P = P_s - P_r$), which is closely linked to piezoelectricity, and a smaller $\Delta P/P_s$ value indicates stronger stability of the long-range ordered ferroelectric domain structures induced by the electric field. As shown in Figure 4D, the PNN-PZ-PT piezoelectric ceramic exhibits a low $\Delta P/P_s$ of 17.5% at room temperature, signifying better stability of its long-range ordered domain configurations, and it is a key factor contributing to its ultrahigh piezoelectric coefficients. However, when the temperature rises to 70 °C, the $\Delta P/P_s$ value abruptly increases to 50%, indicating that elevated temperatures destabilize the long-range ordered domains after electric field removal, and transform into nanoscale domain structures, resulting in reduced polarization intensity and diminished piezoelectric performance.

Local domain structures

Given the pivotal influence of domain structures on the electromechanical performance of ferroelectric materials, domain configurations are critical to elucidating the fundamental mechanisms underlying the high piezoelectricity in PNN-PZ-PT ceramics. PFM was used to map key domain-related features, including surface domain morphology, the local piezoelectric response, and the domain reversal process.

Figure 5A-C presents the PFM amplitude, phase, and three-dimensional (3D) phase-amplitude mappings of the PNN-PZ-PT ceramic, respectively. The 3D phase-amplitude composite map [Figure 5C] integrates the amplitude and phase through color-coded phase information (polarization orientation) and amplitude-modulated surface topography (polarization magnitude), enabling simultaneous visualization of polarization intensity distribution and orientation heterogeneity across the ceramic sample. The PNN-PZ-PT ceramic features irregular nanoscale maze-like domain structures with widths on the hundred-nanometer scale, as evidenced in Figure 5A-C and Supplementary Figure 4.

To further characterize the local polarization disorder of the nanoscale domains in PNN-PZ-PT ceramics, quantitative analysis of the domain patterns using the average autocorrelation function $< C(r) >$, which is defined as[43-46]:

$$\langle C(r)\rangle = \sigma^2 \exp\left[-\left(\frac{r}{\langle \xi \rangle}\right)^{2b}\right] \tag{5}$$

here, the parameters r and b ($0 < b < 1$) are the distance from the central peak and the exponent parameter which represents the roughness of the polarization interface, respectively, while σ is a constant. The $< \xi >$ is the average domain size, representing the degree of polar disorder of the local polarization orientation, where a smaller $< \xi >$ value correlates with enhanced polar disorder. Figure 5D displays the fitting results of the average autocorrelation function, demonstrating excellent agreement with experimental data. Notably, the PNN-PZ-PT ceramic exhibits a smaller $< \xi >$ value of 83 nm, indicating a strong local polarization orientation disorder.

Switching spectroscopy-piezoresponse force microscopy (SS-PFM) was employed to quantitatively investigate nanodomain switching dynamics in the PNN-PZ-PT ceramic, as shown in Figure 5E. It can be clearly observed that the ceramic displays representative local amplitude-voltage and phase-voltage loops at a tip voltage of 8 V, where the characteristic butterfly-shaped amplitude curve and a sharp ~180° phase reversal unequivocally confirm robust nanoscale ferroelectricity with excellent reversible polarization switching under alternating biases. The local piezoresponse (PR) hysteresis loop in Figure 5F was derived using $PR = A \cdot \cos\varphi$, where A denotes the polarization amplitude from the amplitude-voltage loop and φ represents the phase angle extracted from the phase-voltage loop. The loop exhibits highly symmetric ferroelectric hysteresis with pronounced maximum piezoresponse (PR_{max}) and remanent piezoresponse (PR_0) at zero bias, demonstrating spontaneous polarization retention at the nanoscale.

To further understand the domain dynamics under external field, the detailed domain switching process driven by tip voltages was investigated. A 10 μm × 10 μm area is initially poled by tip voltage of 8 V (the left side) and -8 V (the right side) to achieve downward and upward domains, as shown in Figure 6A. The distinct 180° phase contrast reveals that the domain can be easily switched. Subsequently, opposite tip biases of varied values (±2 V, ±4 V, ±6 V, ±8 V) were applied to reverse the domains. The resulting domain patterns were imaged in PFM mode, as illustrated in Figure 6B. It is demonstrated that domain nucleation occurs at -4 and 6 V for the downward-to-upward and upward-to-downward domain reversal processes, respectively. The domain diameter then increases with increasing tip voltage. These results indicate that the PNN-PZ-PT ceramic possesses promising microscale polarization switching and readability, underscoring its robust ferroelectric reversibility at microscales.

It is well-established that piezoelectric materials exhibit macroscopic piezoelectric responses only after electric field poling, making the study of the domain structures post-poling crucial for understanding the origin of high piezoelectric performance. Figure 6C presents the domain configurations of the PNN-PZ-PT ceramic after poling under a 15 kV/cm DC electric field followed by 72 h of aging, and the PFM scanning area is 30 μm × 30 μm. From the PFM amplitude and phase maps, it is evident that most of the scanned regions maintain uniform amplitude intensity and consistent phase values, and only a small fraction of areas exhibits weaker amplitude signals and opposite phase orientations relative to the poling electric field direction (e.g., yellow regions of the phase image in Figure 6C). This observation highlights the ceramic's exceptional polarization switching characteristics, where the DC electric field effectively aligns spontaneous polarization vectors with the electric field direction and stabilizes them.

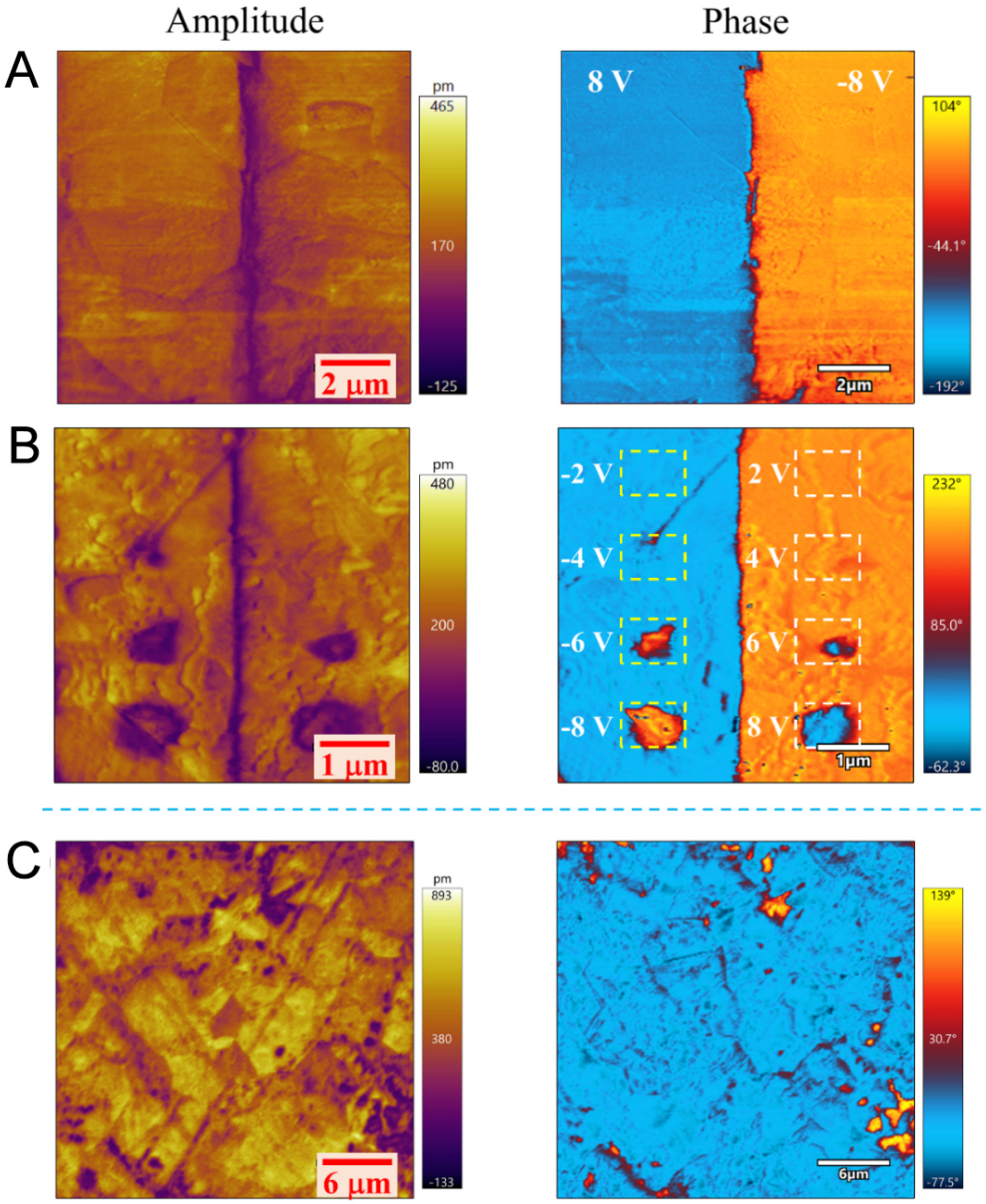


Figure 6. (A and B) PFM images of amplitude switching and phase switching under positive and negative tip DC voltages for the unpoled 0.555PNN-0.145PZ-0.30PT ceramic; (C) PFM images of the 15 kV/cm DC electric field-poled 0.555PNN-0.145PZ-0.30PT ceramic. The domain structure areas in (A), (B), and (C) are 10 μm × 10 μm, 5 μm × 5 μm, and 30 μm × 30 μm, respectively. DC: Direct current; PFM: piezoelectric force microscopy.

Furthermore, the uniform amplitude intensity across the sample suggests that the projected polarization vectors of the domain structures within the testing plane exhibit nearly identical strengths. This uniformity implies a high degree of spontaneous polarization alignment among individual grains in the PNN-PZ-PT ceramic with a high piezoelectric coefficient. Such alignment significantly enhances the collective contribution of polarization vectors to the macroscopic piezoelectric response, serving as a key determinant of the material's outstanding electromechanical performance.

CONCLUSIONS

In summary, the tricritical point composition PNN-PZ-PT ceramics with excellent piezoelectric response were successfully fabricated. The enhanced piezoelectric coefficient is attributed to the synergistic effects of

the high ralative dielectric permittivity and the large remanent polarization. Microstructural analysis revealed that the PNN-PZ-PT ceramic with coexistence of multiple ferroelectric phases contain irregular small-sized maze-like nanodomain structures with strong local disorder, which play a critical role in facilitating polarization alignment and ensuring high stability after poling. These findings demonstrate that constructing strongly disordered nanodomain structures is an effective strategy for achieving exceptional piezoelectric properties in PNN-PZ-PT ceramics.

DECLARATIONS

Authors' contributions

Synthesis and testing of materials, data collection, original manuscript writing: Li, K.; Wang, Q.; Qi, X.
Validation and original manuscript revision: Zheng, L.; Gong, W.
Data collection and analysis: Zhang, D.; Zhou, Y.; Yang, Z.; Zeng, Z.
Chart design: An, Y.
Validation: Zhao, Z.
Revision: Mei, H.
Reviewing and editing: Bian, L.

Availability of data and materials

The raw data supporting the findings of this study are available within this Article and its Supplementary Materials. Further data is available from the corresponding authors upon reasonable request.

AI and AI-assisted tools statement

Not applicable.

Financial support and sponsorship

This research was supported by the Guangdong Basic and Applied Basic Research Foundation (2022A1515110498, 2023A1515140074), the National Natural Science Foundation of China (52302137 and 12474088), the Natural Science Foundation of Shandong province (ZR2022YQ43 and ZR2025QA07), the Guangdong Provincial Department of Education (2021ZDJS080, 2021ZDZX1040), the Professorial and Doctoral Scientific Research Foundation of Huizhou University (2022JB030), and the Innovative Research Team of Guangdong Province & Huizhou University (IRTHZU).

Conflicts of interest

All authors declared that there are no conflicts of interest.

Ethical approval and consent to participate

Not applicable.

Consent for publication

Not applicable.

Copyright

© The Author(s) 2026.

Supplementary Materials

Supplementary Materials

REFERENCES

1. Liu, J.; Zhang, D.; Yan, Y.; Li, Z.; Li, F.; Yang, S. Piezoelectric ceramic hardening through defect distribution optimization in multicomponent systems. *Adv. Funct. Mater.* **2025**, *35*, 2413130. DOI
2. Yan, Y.; Qiao, Y.; Wang, L.; et al. A novel strategy for obtaining lead-based piezoelectric ceramics with giant piezoelectricity and high-temperature stability through the construction of "slush-like" polar states. *J. Mater. Sci. Technol.* **2025**, *221*, 25-35. DOI

3. Qin, H.; Zhao, J.; Chen, X.; et al. Investigation of $BiFeO_3$-$BaTiO_3$ lead-free piezoelectric ceramics with nonstoichiometric bismuth. *Microstructures* **2023**, *3*, 2023035. DOI
4. Yang, L.; Huang, H.; Xi, Z.; et al. Simultaneously achieving giant piezoelectricity and record coercive field enhancement in relaxor-based ferroelectric crystals. *Nat. Commun.* **2022**, *13*, 2444. DOI
5. Lin, J.; Peng, J.; Huang, X.; et al. Tailoring the microstructure of lead-free KNN piezoelectric ceramics for force-sensitive smart windows. *Microstructures* **2025**, *5*, 2025058. DOI
6. Huang, Y.; Zhang, L.; Jing, R.; et al. Lead zirconate titanate-based ceramics with high piezoelectricity and broad usage temperature range. *Chem. Eng. J.* **2023**, *477*, 147192. DOI
7. Wang, P.; Guo, Q.; Li, F.; et al. $Pb(In_{1/2}Nb_{1/2})O_3$-$PbZrO_3$-$PbTiO_3$ ternary ceramics with temperature-insensitive and superior piezoelectric property. *J. Eur. Ceram. Soc.* **2022**, *42*, 3848-56. DOI
8. Bian, L.; Qi, X.; Li, K.; et al. High-performance $Pb(Ni_{1/3}Nb_{2/3})O_3$-$PbZrO_3$-$PbTiO_3$ ceramics with the triple point composition. *J. Eur. Ceram. Soc.* **2021**, *41*, 6983-90. DOI
9. O'Malley, C. J.; Tang, X.; Koval, V.; et al. Unveiling the mechanism of substitution-induced high piezoelectric performance in PLZT ceramics. *J. Adv. Ceram.* **2025**, *14*, 9221097. https://www.sciopen.com/article/10.26599/JAC.2025.9221097 (accessed 2026-02-24).
10. Liu, Y.; Yang, J.; Deng, S.; et al. Flexible polarization configuration in high-entropy piezoelectrics with high performance. *Acta. Mater.* **2022**, *236*, 118115. DOI
11. Li, F.; Lin, D.; Chen, Z.; et al. Ultrahigh piezoelectricity in ferroelectric ceramics by design. *Nat. Mater.* **2018**, *17*, 349-54. DOI
12. Yu, X.; Hou, Y.; Zheng, M.; Zhu, M. High and thermally stable piezoelectricity in relaxor-based ferroelectrics for mechanical energy harvesting. *J. Mater. Chem. A.* **2021**, *9*, 26741-9. DOI
13. Gao, X.; Wu, J.; Yu, Y.; et al. Giant piezoelectric coefficients in relaxor piezoelectric ceramic PNN-PZT for vibration energy harvesting. *Adv. Funct. Mater.* **2018**, *28*, 1706895. DOI
14. Cheng, M.; Zhang, D.; Yan, Y.; Li, Z.; Wang, P.; Murakami, R. Optimizing piezoelectric performance of complex perovskite through increasing diversity of B-site cations. *J. Mater. Sci. Technol.* **2024**, *170*, 78-86. DOI
15. Lee, G.; Kim, J.; Kim, S.; Kwak, S.; Min, B.; Nahm, S. Investigation of the structural and piezoelectric characteristics of $(1-x)Pb(Zr,Ti)O_3$-$xPb(Zn_{0.4}Ni_{0.6})_{1/3}Nb_{2/3}O_3$ ceramics with R-PC-T multistructure. *J. Eur. Ceram. Soc.* **2024**, *44*, 7006-17. DOI
16. Liu, X.; Ren, X.; Tang, M.; Wang, Y.; Xu, Z.; Yan, Y. Superior temperature stability of electromechanical properties and resonant frequency in PYN-PZT piezoelectric ceramics. *J. Eur. Ceram. Soc.* **2024**, *44*, 873-81. DOI
17. Zhang, S. J. High entropy design: a new pathway to promote the piezoelectricity and dielectric energy storage in perovskite oxides. *Microstructures* **2023**, *3*, 2023003. DOI
18. Liu, Y.; Deng, S.; Li, J.; et al. High-performance electrostrictive relaxors with dispersive endotaxial nanoprecipitations. *Adv. Mater.* **2022**, *34*, 2204743. DOI
19. Lee, T.; Lee, H.; Kim, D.; et al. Relation between structure and piezoelectric properties of $(1-x-y)PbZrO_3$-$xPbTiO_3$-$yPb(Ni_{1/3}Nb_{2/3})O_3$ ceramics near triple point composition. *J. Eur. Ceram. Soc.* **2016**, *36*, 4049-57. DOI
20. Lee, T.; Kim, S.; Kim, E.; et al. Crystal structure and piezoelectric characteristics of various phases near the triple-point composition in PZ-PT-PNN system. *J. Eur. Ceram. Soc.* **2020**, *40*, 1947-56. DOI
21. Vittayakorn, N.; Rujijanagul, G.; Tan, X.; Marquardt, M. A.; Cann, D. P. The morphotropic phase boundary and dielectric properties of the $xPb(Zr_{1/2}Ti_{1/2})O_3$-$(1-x)Pb(Ni_{1/3}Nb_{2/3})O_3$ perovskite solid solution. *J. Appl. Phys.* **2004**, *96*, 5103-9. DOI
22. Prakash, H.; Kumar, N.; Kumar, .; A, .; et al. On the origin of high piezoelectric response in $PbNi_{1/3}Nb_{2/3}O_3$-$PbZrO_3$-$PbTiO_3$ ternary system. *J. Mater. Sci. Mater. Electron.* **2025**, *36*, 1639. DOI
23. Guo, F.; Zhang, S.; Long, W.; Fang, P.; Li, X.; Xi, Z. SnO_2 modified PNN-PZT ceramics with ultra-high piezoelectric and dielectric properties. *Ceram. Int.* **2022**, *48*, 23241-8. DOI
24. Yimnirun, R.; Wongmaneerung, R.; Wongsaenmai, S.; Ngamjarurojana, A.; Ananta, S.; Laosiritaworn, Y. Dynamic hysteresis and scaling behavior of hard lead zirconate titanate bulk ceramics. *Appl. Phys. Lett.* **2007**, *90*, 112908. DOI
25. Wang, S.; Li, X.; Wang, J.; et al. Enhanced electromechanical properties in $MnCO_3$-modified $Pb(Ni,Nb)O_3$-$PbZrO_3$-$PbTiO_3$ ceramics via defect and domain engineering. *J. Am. Ceram. Soc.* **2023**, *106*, 1970-1980. DOI
26. Du, J.; Qiu, J.; Zhu, K.; Ji, H. Enhanced piezoelectric properties of $0.55Pb(Ni_{1/3}Nb_{2/3})O_3$-$0.135PbZrO_3$-$0.315PbTiO_3$ ternary ceramics by optimizing sintering temperature. *J. Electroceram.* **2014**, *32*, 234-9. DOI
27. Bokov, A. A.; Ye, Z. Recent progress in relaxor ferroelectrics with perovskite structure. *J. Mater. Sci.* **2006**, *41*, 31-52. DOI
28. Li, K.; Sun, E.; Qi, X.; Yang, B.; Liu, J.; Cao, W. Dielectric relaxation and local domain structures of ferroelectric PIMNT and PMNT single crystals. *J. Am. Ceram. Soc.* **2020**, *103*, 1744-54. DOI
29. Bokov, A.; Ye, Z. Phenomenological description of dielectric permittivity peak in relaxor ferroelectrics. *Solid. State. Commun.* **2000**, *116*, 105-8. DOI

30. Zhang, Y.; Zhu, X.; Zhu, J.; Zeng, X.; Feng, X.; Liao, J. Composition design, phase transitions and electrical properties of Sr^{2+}-substituted *x*PZN-0.1PNN-(0.9-*x*)PZT piezoelectric ceramics. *Ceram. Int.* **2016**, *42*, 4080-9. DOI
31. Glazounov, A. E.; Tagantsev, A. K. Direct evidence for Vögel-Fulcher freezing in relaxor ferroelectrics. *Appl. Phys. Lett.* **1998**, *73*, 856-8. DOI
32. Viehland, D.; Jang, S. J.; Cross, L. E.; Wuttig, M. Freezing of the polarization fluctuations in lead magnesium niobate relaxors. *J. Appl. Phys.* **1990**, *68*, 2916-21. DOI
33. Tagantsev, A. K. Vogel-Fulcher relationship for the dielectric permittivity of relaxor ferroelectrics. *Phys. Rev. Lett.* **1994**, *72*, 1100-3. DOI
34. Liu, G.; Kong, L.; Hu, Q.; Zhang, S. Diffused morphotropic phase boundary in relaxor-$PbTiO_3$ crystals: High piezoelectricity with improved thermal stability. *Adv. Physics. Res.* **2020**, *7*, 021405. DOI
35. Bian, L.; Wang, Q.; Qi, X.; et al. Improved electromechanical properties of $Pb(Ni_{1/3}Nb_{2/3})O_3$-$PbZrO_3$-$PbTiO_3$ ferroelectric ceramics via Sm-modification. *Ceram. Int.* **2024**, *50*, 5739-45. DOI
36. Wang, J. J.; Wang, S. H.; Li, X.; et al. High piezoelectricity and low strain hysteresis in PMN-PT-based piezoelectric ceramics. *J. Adv. Ceram.* **2023**, *12*, 792-802. DOI
37. Zheng, F.; Tian, X.; Fang, Z.; et al. Sm-Doped PIN-PMN-PT transparent ceramics with high Curie temperature, good piezoelectricity, and excellent electro-optical properties. *ACS. Appl. Mater. Interfaces.* **2023**, *15*, 7053-62. DOI
38. Zheng, T.; Wu, H.; Yuan, Y.; et al. The structural origin of enhanced piezoelectric performance and stability in lead free ceramics. *Energ. Environ. Sci.* **2017**, *10*, 528-37. DOI
39. Fu, D.; Taniguchi, H.; Itoh, M.; Koshihara, S. Y.; Yamamoto, N.; Mori, S. Relaxor $Pb(Mg_{1/3}Nb_{2/3})O_3$: a ferroelectric with multiple inhomogeneities. *Phys. Rev. Lett.* **2009**, *103*, 207601. DOI
40. Wieder, H. H. Activation field and coercivity of ferroelectric barium titanate. *J. Appl. Phys.* **1957**, *28*, 367-9. DOI
41. Merz, W. J. Domain formation and domain wall motions in ferroelectric $BaTiO_3$ single crystals. *Phys. Rev.* **1954**, *95*, 690-8. DOI
42. He, W.; Li, Q.; Xi, X.; Yan, Q. High temperature-insensitive ferro-/piezoelectric properties and nanodomain structures of $Pb(In_{1/2}Nb_{1/2})O_3$-$PbZrO_3$- $Pb(Mg_{1/3}Nb_{2/3})O_3$-$PbTiO_3$ relaxor single crystals. *J. Am. Ceram. Soc.* **2018**, *101*, 1236-44. DOI
43. Shvartsman, V. V.; Kleemann, W.; Łukasiewicz, T.; Dec, J. Nanopolar structure in $Sr_xBa_{1-x}Nb_2O_6$ single crystals tuned by Sr/Ba ratio and investigated by piezoelectric force microscopy. *Phys. Rev. B.* **2008**, *77*, 054105. DOI
44. Shvartsman, V. V.; Kholkin, A. L.; Orlova, A.; Kiselev, D.; Bogomolov, A. A.; Sternberg, A. Polar nanodomains and local ferroelectric phenomena in relaxor lead lanthanum zirconate titanate ceramics. *Appl. Phys. Lett.* **2005**, *86*, 202907. DOI
45. He, W.; Carpenter, M. A.; Lampronti, G. I.; Li, Q.; Yan, Q. Local strain heterogeneity and elastic relaxation dynamics associated with relaxor behavior in the single-crystal perovskite $Pb(In_{1/2}Nb_{1/2})O_3$-$PbZrO_3$-$Pb(Mg_{1/3}Nb_{2/3})O_3$-$PbTiO_3$. *Phys. Rev. B.* **2017**, *96*, 144109. DOI
46. He, W.; Li, Q.; Sun, Y.; Xi, X.; Zhang, Y.; Yan, Q. Investigation of piezoelectric property and nanodomain structures for PIN-PZ-PMN-PT single crystals as a function of crystallographic orientation and temperature. *J. Mater. Chem. C.* **2017**, *5*, 2459-65. DOI

Disclaimer/Publisher's Note: All statements, opinions, and data contained in this publication are solely those of the individual author(s) and contributor(s) and do not necessarily reflect those of OAE and/or the editor(s). OAE and/or the editor(s) disclaim any responsibility for harm to persons or property resulting from the use of any ideas, methods, instructions, or products mentioned in the content.



© The Author(s) 2026. Open Access This article is licensed under a Creative Commons Attribution 4.0 International License (https://creativecommons.org/licenses/by/4.0/), which permits unrestricted use, sharing, adaptation, distribution and reproduction in any medium or format, for any purpose, even commercially, as long as you give appropriate credit to the original author(s) and the source, provide a link to the Creative Commons license, and indicate if changes were made.